CRYSTAL GROWTH & DESIGN

Article

pubs.acs.org/crystal

Time-Resolved in Situ Raman Spectroscopy of the Nucleation and Growth of Siderite, Magnesite, and Calcite and Their Precursors

German Montes-Hernandez*[,†,‡] and François Renard[†,‡,§]

[†]CNRS, ISTerre, F-38041 Grenoble, France

[‡]Université Grenoble Alpes, ISTerre, F-38041 Grenoble, France

[§]Department of Geosciences, PGP, University of Oslo, Box 1048, Blindern, 0316 Oslo, Norway

ABSTRACT: The nucleation and growth processes of particles and crystals from aqueous systems are actively investigated and occasionally open to debate because multistep nucleation and prenucleation events often exist. This study demonstrates that time-resolved Raman spectroscopic measurements can provide complementary and useful information on the nucleation and growth of particles and crystals from homogeneous and heterogeneous systems at different pressure−temperature conditions. Three minerals were chosen for this study: siderite, magnesite, and calcite, three carbonate minerals that are widespread in geological environments and have numerous industrial and medical applications. As expected, siderite and calcite can rapidly form via an amorphous precursor when using concentrated solutions of reactants directly mixed at ambient temperature (~25 °C) and pressure (~1 bar) (i.e., via spinodal decomposition or when energetic barrier is close to zero). In addition, calcium carbonate clusters and/or probably also amorphous calcium carbonate (ACC) were detected in the first 5 min prior to calcite nucleation in a $Ca(OH)_2$−H_2O−CO_2 concentrated slurry at 25 °C and 50 bar. The calcite and siderite crystals, nucleated from their respective amorphous phases, grow by oriented aggregation of crystalline nanoparticles leading to porous spherical siderite-mesocrystals or nonporous rhombohedral calcite crystals after 24 h of reaction, as deduced from field emission scanning electron microscopy images and X-ray diffraction analyses. Moreover, the possibility of an Ostwald ripening mechanism contributing to crystal growth is not excluded. Conversely, magnesite formation was not detected by Raman spectroscopy at ambient room temperature; only nesquehonite ($MgCO_3·3H_2O$) and dypingite ($Mg_5(CO_3)_4$−$(OH)_2·5H_2O$) were formed, depending on the reacting solution chemistry. These two minerals transform rapidly into hydromagnesite ($Mg_5(CO_3)_4$−$(OH)_2·4H_2O$) by a heat-aging step at 50 °C. In fact, magnesite formation ($MgCO_3$: anhydrous Mg carbonate) was only measured under hydrothermal conditions (e.g., 90 °C and 50 bar of initial CO_2 pressure), and systematically a transient crystalline phase such as hydromagnesite was observed prior to magnesite nucleation and growth at the investigated conditions. This confirms that crystalline phases (not necessarily polymorphs) can also act as precursors during nucleation and growth of more stable phases. The fact that direct nucleation of magnesite from ionic solutions and slurries at ambient temperature is not observed is probably due to the high level of hydration of Mg ions in aqueous systems.

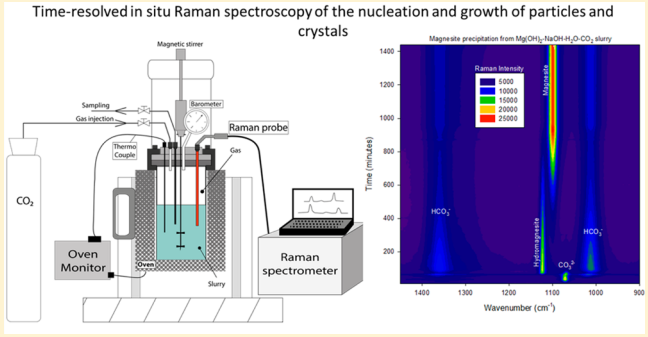

1. INTRODUCTION

The biotic and abiotic formation of carbonate minerals plays a crucial role in the overall carbon cycle. In addition, these minerals often sequester various trace elements of economic importance (actinides and lanthanides), metalloids and heavy metals, and thus control in part their overall cycle. Calcite ($CaCO_3$) is the most common of the anhydrous carbonates, shaping the surface of the Earth in many sedimentary basins and mountain ranges in the form of limestones and marbles.[1−3] Siderite ($FeCO_3$) is a common constituent of low-grade iron-rich sedimentary formations and of some hydrothermal veins; it is found in a broad range of environments including lake sediments, estuaries, carbonate-rich springs, and shallow to deeply buried sediments and rocks.[4,5] Siderite is also a common corrosion product in anoxic artificial environments and has relevance in Fe/CO_2 fuel cells.[6] In contrast to calcite and siderite, magnesite ($MgCO_3$) is quite rare in sedimentary formations; it can easily be formed by the hydrothermal alteration of ultrabasic rocks interacting with rich-carbonate fluids. However, its precipitation at low temperature remains an emblematic question in geosciences because the formation of this mineral is kinetically inhibited by the fast precipitation of hydrated magnesium carbonates such as nesquehonite, dypingite, etc.[7,8] These three minerals are also found in meteorites and suspected or measured in other telluric planets such as Mars and Venus.[9,10] In natural systems, information on their stability,

Received: September 23, 2016
Revised: November 13, 2016
Published: November 15, 2016

ACS Publications © XXXX American Chemical Society

DOI: 10.1021/acs.cgd.6b01406
Cryst. Growth Des. XXXX, XXX, XXX−XXX

polymorphism, chemical composition, biotic or abiotic origin, and mineral coexistence can be of great importance in determining how a given ore deposit has been formed.[11,12] Moreover, these three carbonates have major medical and industrial applications, including CO_2 mineral sequestration.[13−15] In this way, several experimental studies have reported how anhydrous carbonates can nucleate and grow; calcite has been the most investigated mineral, mainly due to its facility to precipitate in a wide range of experimental conditions.[16−20] Precipitation of siderite and magnesite has been widely investigated, even though several experimental studies have been reported.[4,6,8,21,22]

Following these studies, the nucleation and growth processes of anhydrous carbonates, including the influence of impurities (ions or molecules) and additives, represent very active research topics. Some experimental studies in aqueous systems have shown that carbonates can form either along classical crystallization pathways, i.e., by spontaneous nucleation from supersaturated solutions, or by heterogeneous nucleation on pre-existing nucleation sites followed by crystal growth via ion-by-ion or molecule-by-molecule (unit formula) attachment to existing nuclei.[20,23−25] More recently, other studies have also demonstrated that carbonates, in particular, calcite, can form following the so-called nonclassical crystallization pathway. This more complex pathway in homogeneous systems involves first the formation of stable prenucleation clusters from an ionic solution,[19] these clusters quickly being identified as polymer-induced liquid precursors.[26] Following this nonclassical concept, either the clusters aggregate to form amorphous and/or crystalline calcium carbonate, or the amorphous bulk phase nucleation is followed by a rapid transformation into the crystalline bulk phase.[27] Finally, the mesoscale self-assembly of primary nanoparticles or units, often forming so-called mesocrystals, can also be considered in this nonclassical crystallization pathway.[28] The carbonate mesocrystals obtained in this way can finally be rearranged by coalescing into single crystals that may contain macromolecules in their structure.[28−30] Carbonate mesocrystals (e.g., bastnasite: $CeCO_3F$ and siderite) can be formed in the absence of macromolecules or organic additives, but the orientation mechanisms of constituent nanoparticles remain unclear.[31] Recent studies claim that amorphous carbonate nanoparticles do not necessarily serve as direct precursors to anhydrous carbonate nucleation but that direct calcite nucleation can occur concurrently with other hydrated or nonhydrated phases.[20,24,32] In fact, crystalline phases (not necessarily polymorphs) can also act as precursors during nucleation and growth of more stable phases as predicted by the Ostwald step rule. This is the case for magnesite ($MgCO_3$), where hydromagnesite ($Mg_5(CO_3)_4(OH)_2{\cdot}4H_2O$) systematically precedes the hydrothermal formation of magnesite,[8,22,33,34] except at high temperature (>200 °C) where direct magnesite precipitation can occur.[8] The formation of magnesite at ambient temperature (~25 °C) is virtually impossible, or geological time scales are probably required.[35,36] This limitation has been related to the strong solvation shells of magnesium ions in aqueous media;[8,35,36] a similar situation exists for dolomite ($CaMg(CO_3)_2$) at room temperature and atmospheric pressure in laboratory experiments.[35,37] However, the effect of Mg hydration is not an exclusive factor for the inhibition of magnesite and/or dolomite formation. Recent studies claim the existence of a more intrinsic crystallization barrier and the influence of fluid chemistry (e.g., relative size of the constituting cations) that prevents the formation of a long-range ordered crystallographic structures at ambient conditions.[36,37]

In this context, time-resolved in situ measurements by coupling the reaction systems with microscopic, spectroscopic, chromatographic, or diffractometric analytical methods can contribute to a better understanding of the nucleation and growth processes of particles and crystals.[8,16,38] In the present study, time-resolved Raman spectroscopic measurements are developed to study carbonate formation from agitated slurries under ambient and hydrothermal conditions and provide key insights for a better understanding of the nucleation and growth processes of siderite, magnesite, and calcite. This technique is a powerful means of monitoring reactions in aqueous, organic, and multiphase media at high pressure and temperature.[8,39,40] The experimental setup of this study involved, in particular, the coupling of Raman spectroscopy (immersed probe) with a reaction cell (autoclave) in order to monitor the solution chemistry (e.g., carbonate speciation) and the nucleation and growth processes of mineral particles. This technique provides time-resolved reliable information on the solution chemistry (carbonate speciation) and a realistic assessment of mineral composition of the first nucleating/precipitating particles from agitated solutions (homogeneous systems) and slurries (heterogeneous systems). To the authors' knowledge, this is not possible using other laboratory-based analytical techniques under the experimental conditions considered (up to 100 °C and 100 bar). By conducting an extensive study of the formation of major carbonate minerals under various aqueous conditions, the main aim of the present study is to demonstrate the high potential of time-resolved, in situ Raman spectroscopy to study nucleation and growth mechanisms. This technique could be further developed to study both fundamental questions and engineering applications where carbonates and other minerals are involved.

2. MATERIALS AND METHODS

The formation of siderite, magnesite, and calcite was monitored using a Raman probe (785 nm infrared laser) immersed in a hydrothermal autoclave with an internal volume of 0.6 L. In this experimental setup, the temperature (up to 300 °C), gas pressure (up to 300 bar), and agitation rate (up to 500 rpm) can be regulated independently. Raman spectra were collected by a RAMAN RXN1, Kaiser Optical Systems. In general, an exposure time of 3 s (or 2 s) was used, averaged over three (or two) scans with the delay between successive acquisitions being varied between 6 s and 1 h, depending on the investigated reaction. This means that the system can monitor chemical reactions occurring from 5 s (minimal time) to several days. This is well adapted to the investigated several systems (see below). All data were saved directly on the control computer. Figure 1 shows a schematic illustration of the experimental setup (panel a) and one application example (panel b) displaying the kinetics of CO_2 capture in a concentrated NaOH solution (1 mol/L) and the time-dependent change in carbonate speciation.

2.1. Siderite Formation. An alkaline carbonate solution was first prepared by the simple carbonation of a concentrated NaOH solution (1 mol/L) using compressed CO_2 (initial pressure: 50 bar). On the basis of in situ Raman spectroscopy measurements (see Figure 1b), the carbonation reaction can be written as follows:

$$NaOH + CO_{2(aq)} \rightarrow Na^+ + HCO_3^- \quad (1)$$

During the NaOH solution carbonation process, the carbonate species CO_3^{-2} is initially detected, but is rapidly protonated to form HCO_3^-, which is the dominant carbonate species at the end of the experiment. Aqueous CO_2 was also measured until a macroscopic equilibrium was reached, i.e., when the Raman intensity remains

DOI: 10.1021/acs.cgd.6b01406
Cryst. Growth Des. XXXX, XXX, XXX−XXX

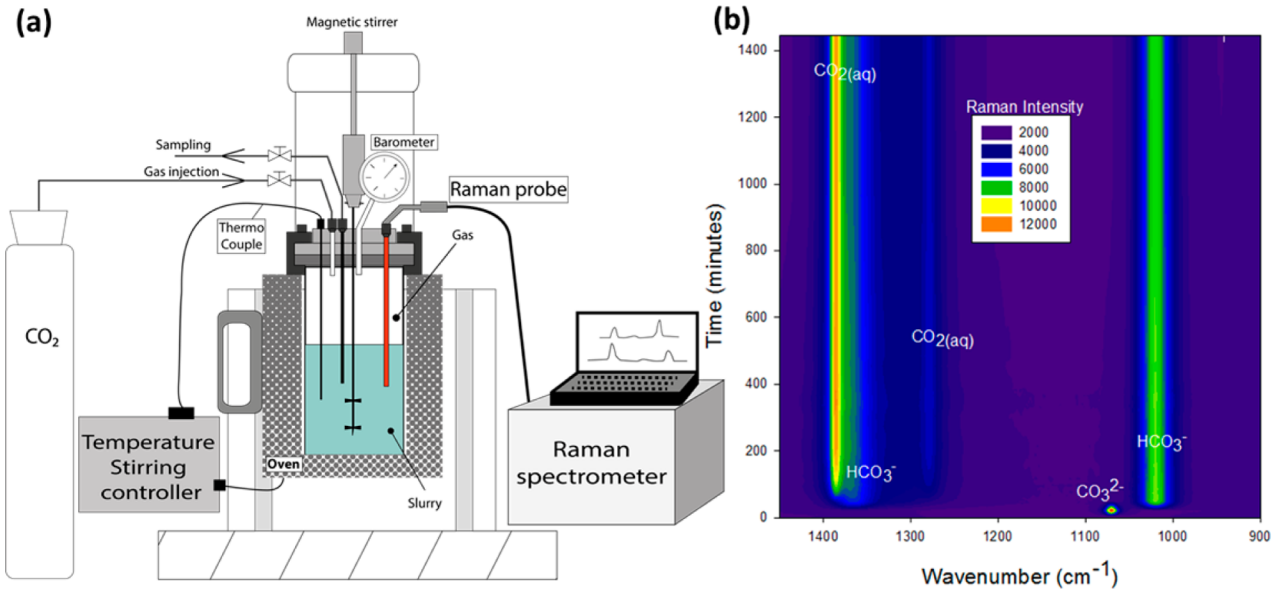

Figure 1. (a) Experimental setup including a batch-reactor (autoclave) coupled with Raman spectroscopy. (b) Time-resolved Raman spectroscopy monitoring of CO_2 capture in a concentrated NaOH solution (1 mol/L) where CO_2 was injected in excess (initial CO_2 pressure = 50 bar) at time = 0 min. The Raman signal detects the time-dependent change in the concentrations of CO_3^{2-}, HCO_3^-, and $CO_{2(aq)}$.

Table 1. Summary of Main Homogeneous and Heterogeneous Systems Relating to the Formation of Fe(II), Mg, and Ca Carbonates from Solutions and Slurries

system	$P-T$ conditions	precipitating phases	nucleation-event time	crystal growth mechanism
$FeCl_2-HCO_3^-$ (homogeneous)	P_{atm}, 25 °C	AFC	spontaneous condensation	precursor
		siderite	9.4 min	oriented aggregation and Ostwald ripening
$CaCl_2-HCO_3^-$ (homogeneous)	P_{atm}, 25 °C	ACC	spontaneous condensation	precursor
		calcite	1[a] min	oriented aggregation and Ostwald ripening
$Ca(OH)_2-H_2O-CO_2$ (heterogeneous)	P_i = 50 bar of CO_2, 25 °C	calcium carbonate clusters	3 min	precursor
		ACC	4–5 min	precursor
		calcite	5 min	molecule-by-molecule addition[b] and Ostwald ripening
$MgCl_2-CO_3^{2-}$ (homogeneous)	P_{atm}, 25 °C	AMC	spontaneous condensation	precursor
		nesquehonite	16 min	precursor
		dypingite	18 h	dissolution–precipitation pathway[c]
$Mg(OH)_2$-NaOH$-H_2O-CO_2$ (heterogeneous)	P_i = 50 bar of CO_2, 25 °C	nesquehonite	105 min	molecule-by-molecule addition[d]
$Mg(OH)_2-H_2O-CO_2$ (heterogeneous)	P_i = 50 bar of CO_2, 25 °C	nesquehonite	40 min	molecule-by-molecule addition[d]
$MgCl_2-HCO_3^-$–NaOH (homogeneous)	P_{atm}, 25 °C	nesquehonite	40 min	molecule-by-molecule addition[e]
$Mg(OH)_2-NaOH-H_2O-CO_2$ (heterogeneous)	P_i = 50 bar of CO_2, 90 °C	hydromagnesite	60 min	precursor
		magnesite	240 min	dissolution–precipitation pathway[f]

[a]When rotational and translational vibrational modes are both detected; P_i: initial pressure of CO_2 (anisobaric conditions). [b]Classical growth nourished by $Ca(OH)_2$ dissolution and aqueous CO_2 forming $CaCO_3^0$ molecules. [c]Progressive dissolution of nesquehonite to nourish progressive precipitation of dypingite and its growth by molecule-by-molecule addition. [d]Classical growth nourished by $Mg(OH)_2$ dissolution and aqueous CO_2 forming nesquehonite-like molecules. [e]Classical growth nourished from ionic solution containing Mg and carbonate species. [f]Progressive dissolution of hydromagnesite to nourish progressive precipitation of magnesite and its growth by molecule-by-molecule addition.

constant for HCO_3^- and the aqueous CO_2. The dissolved CO_2 is instantaneously removed when the reactor is depressurized. This fast degassing step also removes the dissolved oxygen and thus limits the oxidation of Fe(II). The synthesized carbonate solution (300 mL) containing mainly HCO_3^- was then mixed directly with 10 g of ferrous chloride ($FeCl_2$: Sigma-Aldrich with purity >99%). This highly soluble salt is instantaneously dissolved, and the released iron immediately forms ferrous carbonate as visually attested by CO_2 gas being expelled and as measured by a broad Raman peak at 1098 cm^{-1} after about 1 min of reaction. Its fast transformation into crystalline siderite was then monitored for 24 h using spectral acquisition time of 10 s or 1 min. Two reaction temperatures (ambient $T \approx 25$ and 90 °C) were investigated, and these experiments were repeated to confirm the reproducibility of the results.

2.2. Calcite Formation via Amorphous Calcium Carbonate (ACC) Transformation. Similarly to siderite, an alkaline carbonate

DOI: 10.1021/acs.cgd.6b01406
Cryst. Growth Des. XXXX, XXX, XXX–XXX

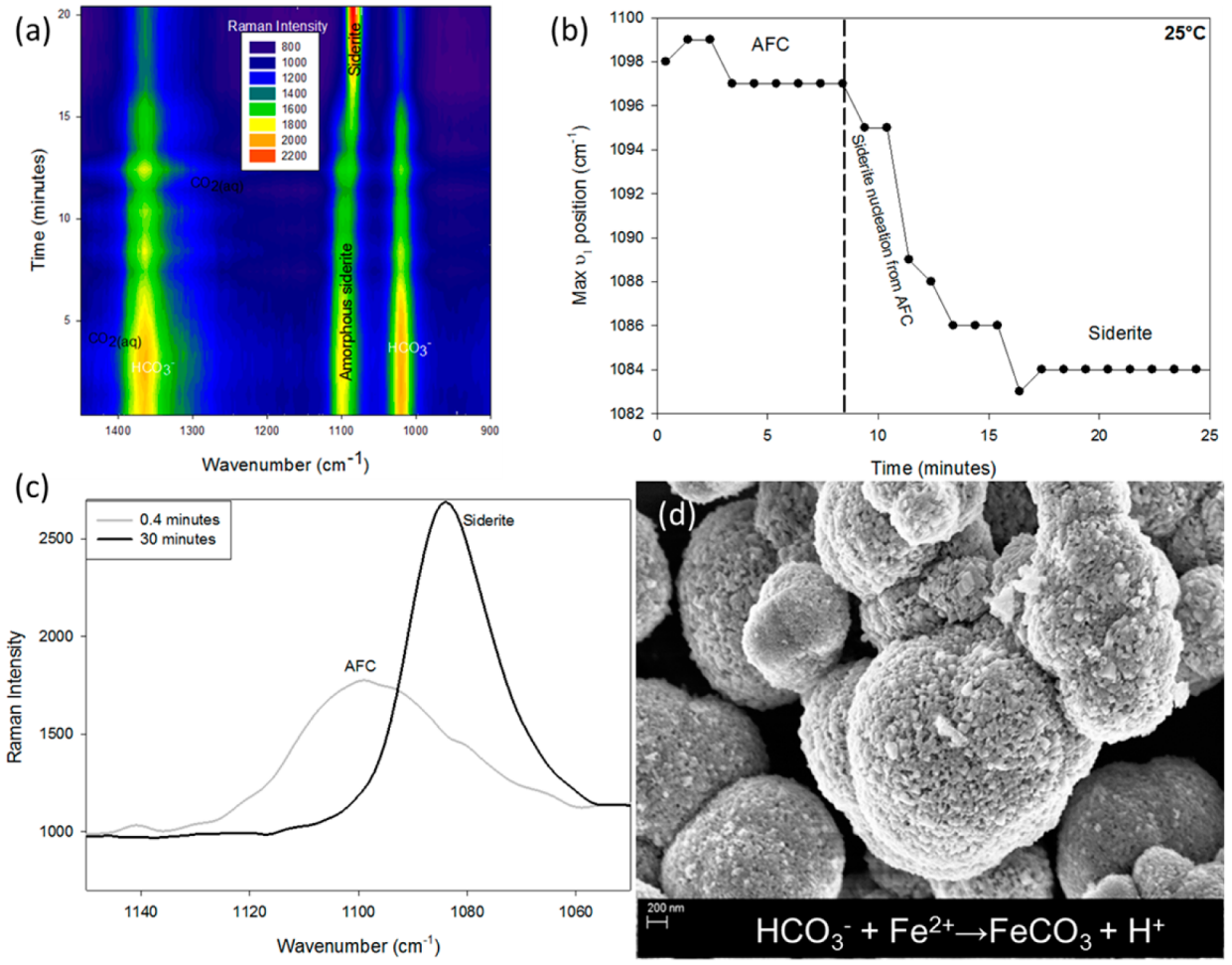

Figure 2. (a) Kinetic behavior of carbonate species (HCO_3^-, $CO_{2(aq)}$) and condensate ferrous carbonate (υ_1 vibration mode) from time-resolved Raman spectroscopy monitoring. (b) Time-dependent variation in the position of the maximum of the peak υ_1 showing amorphous ferrous carbonate (AFC) persistence and a siderite nucleation event. (c) Position of the peak of the υ_1 vibration mode of AFC (1100 cm^{-1}) and siderite (1060 cm^{-1}) crystallized from AFC. (d) Scanning electron image of siderite mesocrystals recovered after 24 h of reaction.

solution was synthesized by carbonation of a concentrated NaOH solution (see also reaction 1). Then, 300 mL of synthesized carbonate solution (HCO_3^-) was mixed directly with 20 g of calcium chloride dihydrate ($CaCl_2 \cdot 2H_2O$: Sigma-Aldrich, with purity >99%). Like the siderite system, this mixture led to the spontaneous condensation of ACC as measured by a Raman peak at 1080 cm^{-1} which is typical for ACC. Its transformation into calcite is very fast, and direct calcite precipitation probably also exists at these conditions,[32] but could not be measured in the experimental setup used.

$$Ca^{2+} + HCO_3^- \rightarrow CaCO_{3(amorphous)} + H^+ \rightarrow CaCO_{3(calcite)} + H^+ \quad (2)$$

Despite this fast transformation, time-resolved Raman spectroscopy measurements with a spectral acquisition time of 10 s were taken to detect such a transformation at ambient temperature (~25 °C).

2.3. Calcite Precipitation from Aqueous Carbonation of a $Ca(OH)_2$ Slurry. A concentrated $Ca(OH)_2$ slurry (1 mol/L) was prepared using 300 mL of high-purity water with an electrical resistivity of 18.2 MΩ cm and 23 g of commercial calcium hydroxide provided by Sigma-Aldrich, with chemical purity of 96%. The calcium hydroxide particles were immediately dispersed by mechanical agitation (400 rpm) and gaseous CO_2 (provided by Linde Gas S.A.) was then injected at 50 bar into the reactor at room temperature (~25 °C) for ~2 min. Following injection, the carbonate speciation and the precipitation of particles were immediately monitored for 24 h by Raman spectroscopy with a 6 s or 10 s acquisition time.

2.4. Magnesite Precipitation. Magnesite precipitation from the $Mg(OH)_2$–NaOH–H_2O–CO_2 slurry was monitored by Raman measurements at 90 °C and 50 bar of initial CO_2 pressure. In this experiment, 21 g of $Mg(OH)_2$, provided by Sigma-Aldrich with a chemical purity of 99%, 24 g of NaOH, and 300 mL of high-purity water were mixed in the reactor. The slurry was immediately dispersed by mechanical agitation (400 rpm) and CO_2, provided by Linde Gas S.A., was then injected at 50 bar into the reactor at room temperature (~25 °C) for ~3 min. Following injection, the system was heated to 90 °C, and the carbonate speciation and precipitated particles were immediately monitored by Raman spectroscopy for 24 h, with a 1 min spectral acquisition time.

These experiments were also performed at ambient temperature (~25 °C), and two scenarios were tested: (i) absence of NaOH in the system, and (ii) heat-aging step from 25 to 50 °C after stabilization, i.e., after 24 h of reaction at ambient temperature. This simple heat-aging step allows the fast and direct transformation of nesquehonite into hydromagnesite.

2.5. Precipitation of Hydrated Mg-Carbonate via an Amorphous Precursor. A total of 300 mL of a concentrated Na_2CO_3 solution (1 mol/L) was mixed directly with 30 g of $MgCl_2 \cdot 6H_2O$ salt. Like the ACC, this mixture led to the spontaneous condensation of amorphous magnesium carbonate (AMC), as measured by a Raman peak at 1084 cm^{-1} in the first 15 s. Its transformation into nesquehonite and other hydrated Mg-carbonates was then monitored for 6 days at ambient temperature (~25 °C). AMC remains detectable by Raman for several minutes; for this simple reason, monitoring was

DOI: 10.1021/acs.cgd.6b01406
Cryst. Growth Des. XXXX, XXX, XXX–XXX

performed with a spectral acquisition time of 1 min for the first 5 h and 15 min for the following 6 days.

2.6. Ex Situ Characterization of Precipitates. In additional to in situ Raman measurements, two other analytical techniques were used in order to characterize the mineral composition, particle size, and crystal morphology of recovered particles after separation from solution, washing, and drying. X-ray powder diffraction (XRD) analyses were performed using a Siemens D5000 diffractometer in Bragg−Brentano geometry, equipped with a theta−theta goniometer with a rotating sample holder. The XRD patterns were collected using Cu kα_1 ($\lambda_{k\alpha1}$ = 1.5406 Å) and kα_2 ($\lambda_{k\alpha2}$ = 1.5444 Å) radiation in the range 2θ = 10−70° with a step size of 0.04° and a counting time of 6 s per step. For high resolution imaging, the solid products were dispersed by ultrasonic treatment in absolute ethanol for 5−10 min. One or two droplets of the suspension were then deposited directly on an aluminum support and coated with platinum. The morphology of the crystals was imaged using a Zeiss Ultra 55 field emission gun scanning electron microscope (FESEM) with a maximum spatial resolution of approximately 1 nm at 15 kV.

3. RESULTS AND DISCUSSION

Calcite and magnesite precipitation was investigated previously in our group using conventional ex-situ characterizations.[14,22,25,41] The present study provides new insights into the reaction mechanism and formation kinetics deduced from in situ Raman monitoring, including the role of the so-called precursors and/or transient condensate phases. In contrast to calcite and siderite, magnesite has not nucleated at ambient temperature due to the high level of Mg ion hydration and probable also due to the existence of a more intrinsic crystallization barrier and the influence of fluid chemistry (e.g., relative size of the constituting cations) that prevents the formation of a long-range ordered crystallographic structures at ambient conditions.[36,37] In the present study, the use of NaOH as sequestering CO_2 agent enables the formation of magnesite at 90 °C in only 24 h.

Assuming that siderite, calcite, and magnesite minerals present significant differences, their formation mechanism and kinetics are summarized in Table 1. In the following paragraphs, each mineral is presented separately.

3.1. Siderite Formation from Amorphous Ferrous Carbonate (AFC). This mineral can form in a wide temperature range, from ambient to 200 °C in alkaline carbonate solutions. However, little is known about the nature of the first precipitating particles, the role of amorphous ferrous carbonate and/or other precursors, and the reaction kinetics.[21] For example, recent studies have suggested that the AFC precursor provides a low-energy pathway for siderite crystallization.[6] Assuming this hypothesis to be true, time-resolved Raman monitoring has confirmed that adding ferrous chloride salt ($FeCl_2$) to a concentrated HCO_3^- solution (1 mol/L) leads to the spontaneous condensation of amorphous ferrous carbonate ($Fe^{2+} + HCO_3^- \rightarrow FeCO_{3(amorphous)} + H^+$) as attested by a broad peak at 1098 cm^{-1}, corresponding to the υ_1 vibration mode (Figure 2c) and the absence of crystal lattice vibration modes (active at lower wavenumbers (300−200 region)). This transient condensate phase persists for about 10 min in the system prior to siderite nucleation from AFC, as reflected by a progressive shifting and thinning of the υ_1 vibration mode peaking at 1084 cm^{-1} after about 17 min of reaction (see Figure 2b,c) and the detection of crystal lattice vibration modes peaking at 283 cm^{-1} (libration mode) and 206 cm^{-1} (translation mode). The low intensity and broad Raman signature is mainly related to nanosized particles (<100 nm) as observed by FESEM. The υ_1 peak position then shifts slightly from 1084 to 1085.5 cm^{-1} after 24 h of reaction. During this period from 20 min to 24 h, periodic intensity variations and slight progressive thinning of υ_1 peak were monitored (see Figure 3), probably indicating a crystal growth process by Ostwald ripening. However, these intriguing periodic intensity variations for the υ_1 peak displayed in Figure 3 could also be

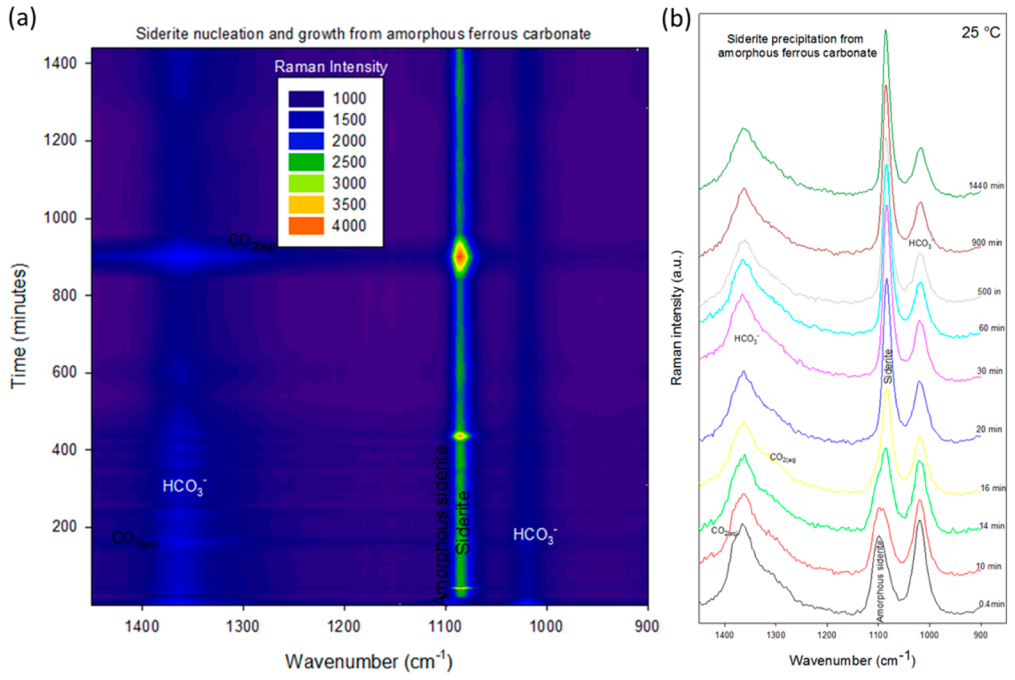

Figure 3. Nucleation and growth processes of siderite from AFC (υ_1 vibration mode) deduced from time-resolved Raman spectroscopy monitoring. (a) Color plot displaying Raman spectroscopy intensity variation with time for precipitates and carbonate species. Figure 2a shows a zoom between 0 and 20 min. (b) Single Raman spectra in the range 1450−900 cm^{-1} extracted at different times.

DOI: 10.1021/acs.cgd.6b01406
Cryst. Growth Des. XXXX, XXX, XXX−XXX

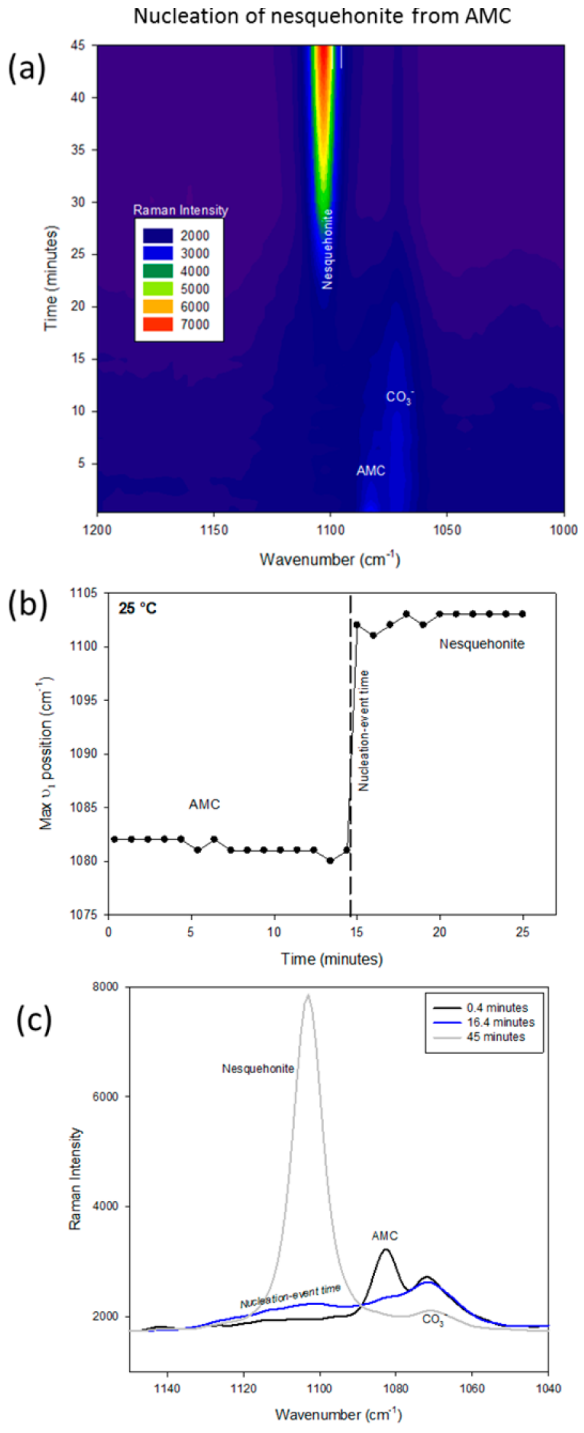

Figure 4. (a) Time-resolved Raman spectroscopy monitoring of nesquehonite nucleation from amorphous magnesium carbonate (AMC) by mixing $MgCl_2$ in a Na_2CO_3 solution (1 mol/L) at 25 °C. (b) AMC persistence and nesquehonite nucleation-event time. (c) Raman spectra showing ν_1 vibrational mode for AMC and nesquehonite.

related to the siderite nanoparticle oriented aggregation events. In effect, oriented aggregation of crystalline nanoparticles is suggested, based on the high resolution FESEM images on recovered precipitates after 24 h of reaction. Such images clearly show micrometer-size spherical aggregates (e.g., inset in Figure 2) composed of crystalline siderite nanoparticles (size <100 nm) as confirmed by the XRD technique (ex-situ) and in

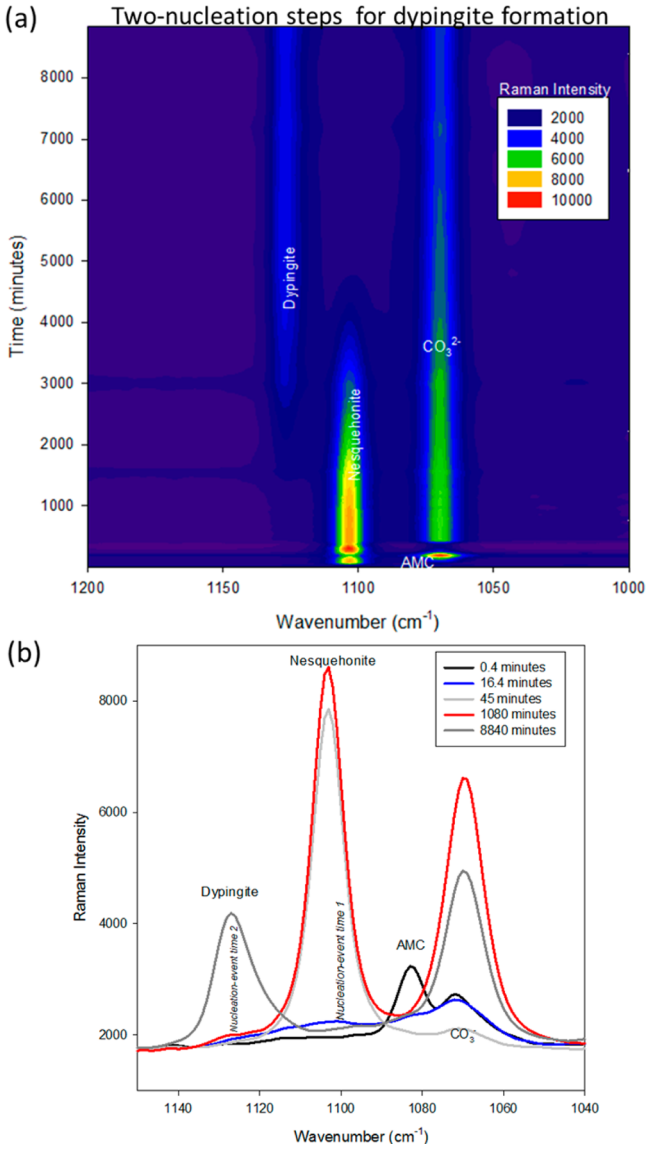

Figure 5. Dypingite formation by two sequential nucleation and dissolution events of (i) AMC and (ii) nesquehonite. (a) Time-resolved Raman spectroscopy monitoring at 25 °C for 6 days; (b) single Raman spectra in the range 1150−1040 cm^{-1} at different times.

situ Raman. As a consequence, we consider that these data (broad Raman peak, nanoparticles of siderite, and aggregation of them into micrometer-size aggregates) provide three types of circumstantial evidence that, together, point to a self-assembly aggregation process, whose mechanism remains to be understood.

In summary, the Raman monitoring data reveal a complex kinetic behavior during siderite crystallization from AFC. In the present study, a siderite nucleation event was detected after about 10 min of reaction, and the complete transformation of AFC into siderite takes place in only 7 min. Oriented aggregation (leading to siderite mesocrystals) and Ostwald ripening mechanisms are proposed as the main processes of crystalline siderite growth at the investigated conditions.

3.2. Magnesite Formation. The high hydration potential of Mg ions in aqueous media contributes to the inhibition of magnesite precipitation at low temperature. High hydroxyl and/or carbonate alkalinity, salinity, and temperature can

DOI: 10.1021/acs.cgd.6b01406
Cryst. Growth Des. XXXX, XXX, XXX−XXX

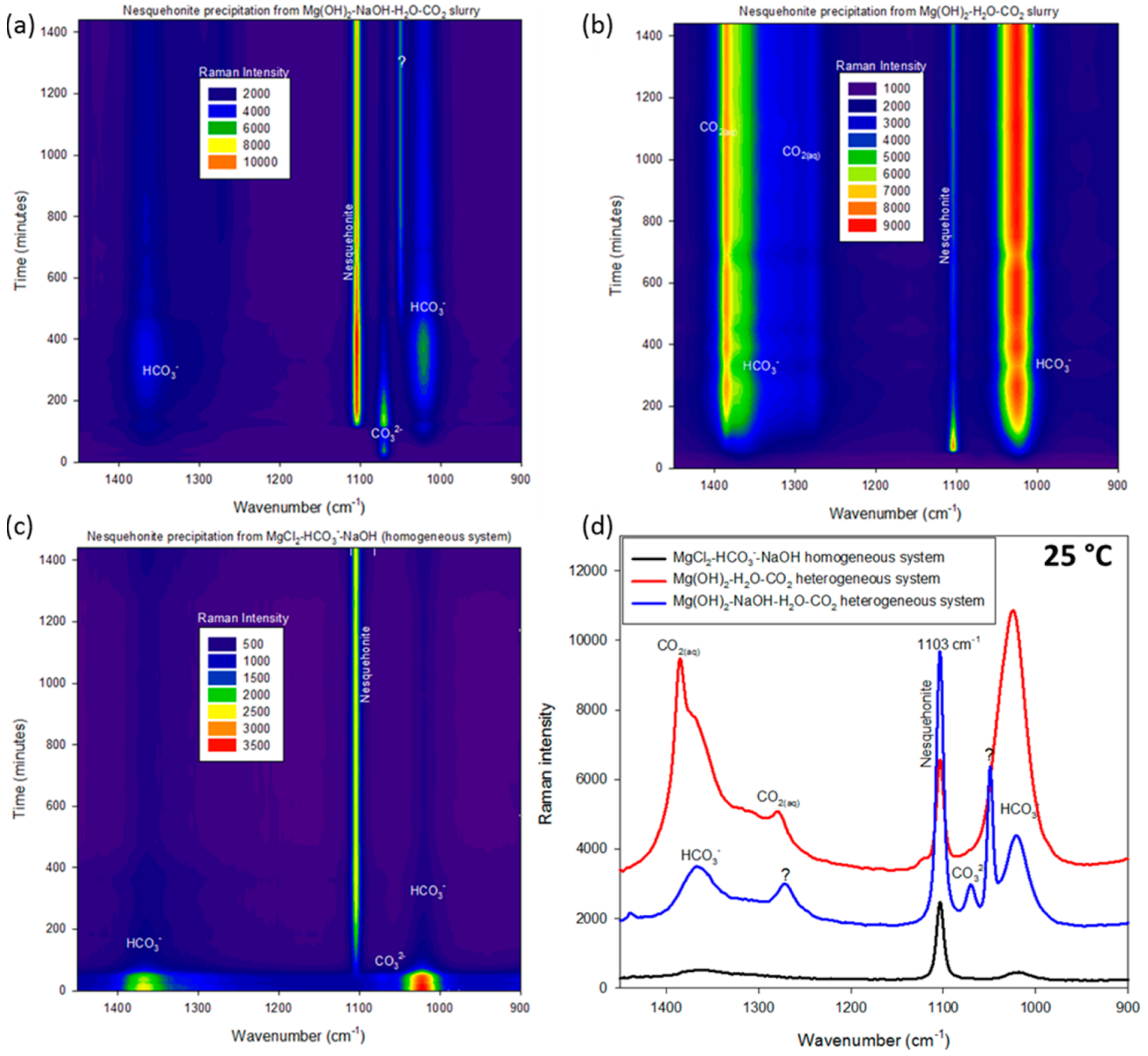

Figure 6. Time-resolved Raman spectroscopy monitoring of the nucleation and growth of nesquehonite at 25 °C from three different reaction systems. (a) $Mg(OH)_2$−NaOH−H_2O−CO_2 slurry. (b) $Mg(OH)_2$−H_2O−CO_2 slurry. (c) $MgCl_2$−HCO_3^-−NaOH homogeneous solution. (d) Single Raman spectra after 24 h min for the three systems.

reduce the hydration potential of Mg ions.[22,42] Assuming this criterion, in the present study, various reaction scenarios (see Table 1) were assessed using Raman monitoring in order to determine the nature of precipitating phases, their persistence in the system over laboratory time scales, and the nucleation events. For example, spontaneous condensation of amorphous magnesium carbonate (AMC) (spinodal decomposition or when the energy barrier to form condensate matter is close to zero) was measured by Raman spectroscopy after 24 s (see Figure 4c). The vibration ν_1 mode peaking at 1082 cm^{-1} is interpreted as AMC that was progressively consumed (decrease in Raman intensity) for 15 min before nucleation of nesquehonite (see Figure 4). Nesquehonite ($MgCO_3{\cdot}3H_2O$) was only a transient phase in the system enabling the nucleation (second nucleation step) of dypingite ($Mg_5(CO_3)_4$−$(OH)_2{\cdot}5H_2O$) after about 18 h of reaction, with a υ_1 peak position at 1127 cm^{-1}, as shown in Figure 5b. In this case, dypingite grows by progressive consumption of nesquehonite as revealed by a decrease in its Raman intensity (see Figure 5a). In other words, these data show that the dissolution of nesquehonite particles nourishes the dypingite growth with a less stable crystalline phase dissolving to nourish a more stable crystalline phase (not necessarily a polymorph) via dissolution−precipitation reactions. This is an example of two nucleation steps where a crystalline phase serves as a precursor for a more stable phase at a given reaction temperature. Conversely, nesquehonite formed at 25 °C is not necessarily or systematically transformed into dypingite. Three other reaction scenarios have shown that nesquehonite peaking at 1103 cm^{-1} (vibration ν_1 mode) can remain stable at the investigated reaction times (24−72 h) and at ambient temperature (~25 °C) (see Figure 6). In fact, only the nucleation time is clearly different, and growth is probably accompanied by the dissolution processes when brucite was used as Mg source (Figure 6a,b) because the Raman intensity for ν_1 vibration mode reaches a transient maximum intensity followed by a decrease and stabilization with time. Conversely, in a homogeneous system

DOI: 10.1021/acs.cgd.6b01406
Cryst. Growth Des. XXXX, XXX, XXX−XXX

($MgCl_2$–HCO_3^-–NaOH), nesquehonite nucleates and grows in a more conventional way, as demonstrated by the progressive increase in Raman intensity until its stabilization with time after a nucleation event (Figure 6c).

It is well-known that an increase in temperature modifies the chemical stability of Mg-hydrated carbonates in aqueous systems; however, their stability and persistence also depend on the chemistry of the interacting solution. For example, nesquehonite formed from brucite carbonation using NaOH as a CO_2 capturing agent is rapidly transformed into hydromagnesite (υ_1 peaking at 1124 cm^{-1}) and magnesite (minor proportion, υ_1 peaking at 1097 cm^{-1}) when it is heat-aged from 25 to 50 °C for 24 h (see Figure 7a). The progressive decrease in Raman intensity for the υ_1 vibration mode of the carbonate group suggests a dissolution–reprecipitation pathway. Conversely, nesquehonite formed at the same temperature, in the absence of NaOH as a capturing agent, remains stable, and the dissolved Mg ions precipitate as additional nesquehonite (υ_1 peaking at 1103 cm^{-1}) and hydromagnesite (minor proportion, υ_1 peaking at 1123 cm^{-1}), as attested by an increase in their Raman intensity. This is also supported by the consumption of bicarbonate ions (HCO_3^-) formed during brucite carbonation at 25 °C. For this particular case, the nesquehonite coexists with hydromagnesite at 50 °C at the end of the experiment. These simple examples confirm the crucial role of the chemistry of the interacting fluid during the formation of Mg carbonates and show that temperature is not an exclusive control parameter for carbonate precipitation. Magnesite (anhydrous carbonate: $MgCO_3$) was thus already synthesized at 90 °C using NaOH as the CO_2 capturing agent.[22] In the present study, time-resolved Raman measurements reveal a precise reaction mechanism of magnesite formation from brucite carbonation using NaOH as the CO_2 capturing agent ($Mg(OH)_2$–NaOH–H_2O–CO_2 system). As expected, two nucleation steps were clearly monitored after CO_2 absorption and its dissociation in the system (see Figure 8). First, hydromagnesite (υ_1 peaking at 1123 cm^{-1}) was nucleated after about 60 min followed by the nucleation of magnesite (υ_1 peaking at 1098 cm^{-1}) after 240 min of reaction. In this case, hydromagnesite serves as a precursor, lowering the energy barrier for magnesite nucleation at moderate temperature (90 °C). Magnesite growth is then nourished by progressive dissolution of hydromagnesite until complete consumption, as attested by a progressive decrease in its υ_1 Raman intensity (Figure 8a). Consequently, magnesite reaches a maximum υ_1 Raman intensity after about 900 min of reaction and seems to be in equilibrium with the interacting carbonate solution (Figure 8). This is another example where a crystalline phase (hydromagnesite: $Mg_5(CO_3)_4(OH)_2{\cdot}4H_2O$) serves as a precursor to form a more stable phase (magnesite: $MgCO_3$) at moderate temperature (90 °C). Note that magnesite is known to precipitate at higher temperatures (>120 °C), and several hours and days are frequently required,[34] whereas here the precipitation is much faster (only 15 h required). Lower temperature and lower synthesis durations for magnesite could have relevant interest for the permanent storage of CO_2 in carbonates when brucite comes from ultrabasic rocks.[34]

3.3. Calcite Formation. In the present study, concentrated ionic solutions were voluntarily used in order to form amorphous calcium carbonate (ACC) spontaneously (spinodal decomposition) as expected to occur at high supersaturations, and the rapid transformation into calcite can thus be monitored by a Raman probe immersed in the suspension. Calcite (ν_1 peaking at 1089 cm^{-1}) and ACC (ν_1 peaking at 1079 cm^{-1}) were

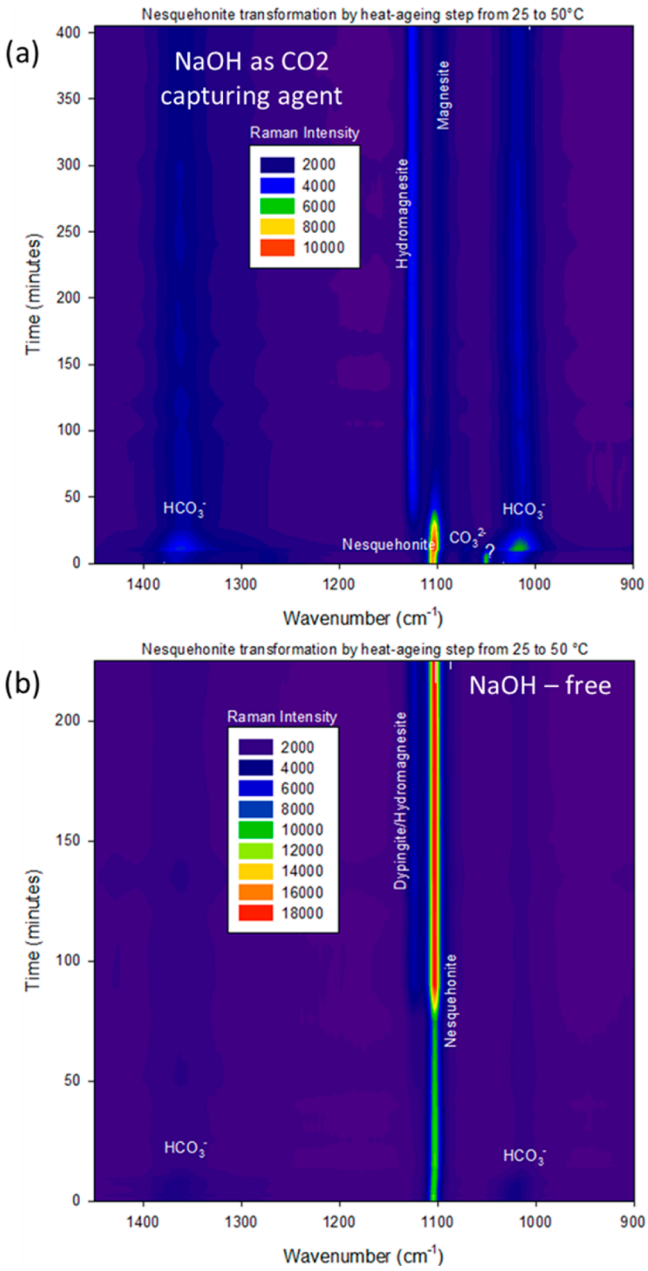

Figure 7. Time-resolved monitoring of nesquehonite transformation by heat-aging step from 25 to 50 °C. (a) Nesquehonite precipitation from brucite carbonation using NaOH as a CO_2 capturing agent at 25 °C. (b) Nesquehonite precipitation from aqueous carbonation of brucite ($Mg(OH)_2$–H_2O–CO_2 system) at 25 °C and degassed prior to heat-aging step.

effectively detected after 10 s (see Figure 9a). However, the librational/rotational and, more particularly, the translational vibration modes (lattice vibration modes) for calcite, are not clearly detected at this monitored time. This supports the fact that calcite nanoparticles coexist with ACC in the first minute of reaction and the first particles precipitated (e.g., calcite nanoparticles and ACC) are metastable; i.e., they can dissolve or transform (ACC particularly) in short times. After 1 min, an effective calcite nucleation event from ACC-calcite nanoparticle bulk phases was thus monitored as attested by the clear detection of two lattice vibrational modes (a librational mode peaking at 283 cm^{-1} and a translational mode peaking at

DOI: 10.1021/acs.cgd.6b01406
Cryst. Growth Des. XXXX, XXX, XXX–XXX

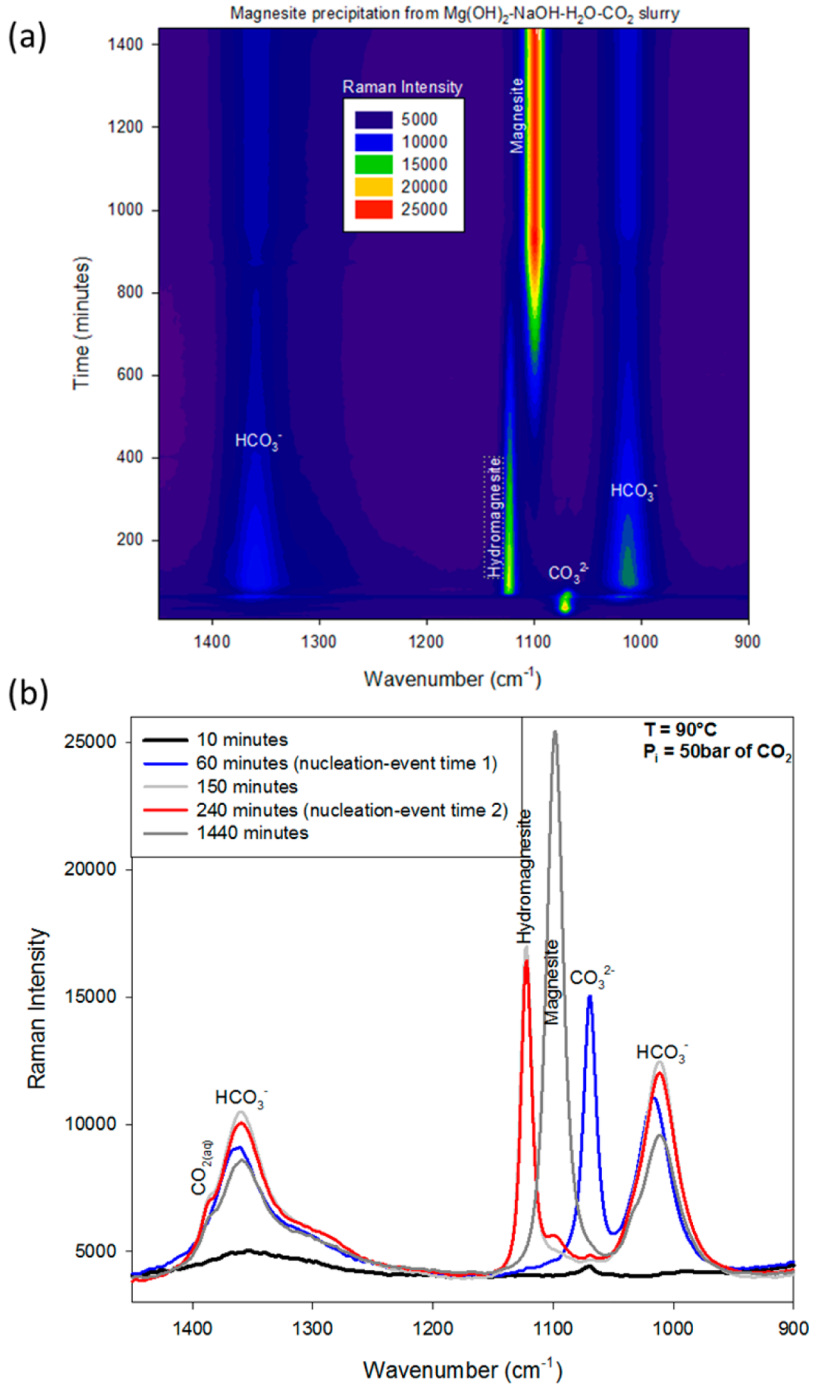

Figure 8. Time-resolved Raman spectroscopy monitoring during nucleation and growth of magnesite from $Mg(OH)_2$−NaOH−H_2O−CO_2 slurry at 90 °C. (a) Kinetic behavior and reaction mechanism revealing hydromagnesite as a transient phase that could act as a crystalline precursor. (b) Raman spectra displaying two-step nucleation events during magnesite formation.

157 cm^{-1}). Their Raman intensity values increased with time and the peak position was slightly shifted during the experiment; in particular, the librational mode shifted from 283 to 285 cm^{-1}. On the other hand, the ACC remained detectable in the system for about 5 min. This means that calcite grows from ACC consumption in the first 5−10 min. It subsequently grows by oriented aggregation of crystalline calcite nanoparticles, as suggested by the nonclassical crystallization pathway and as also deduced from FESEM observations that show noncontinuous layers at the grain scale (see Figure 9b). However, crystal growth by Ostwald ripening process cannot be excluded.

In summary, the values measured in this study suggest that oriented aggregation and Ostwald ripening mechanisms can take place simultaneously during calcite crystal growth when ACC exists or when it is voluntarily used as precursor. The formation of so-called clusters and ACC prior to calcite nucleation is still a debated question.[27,43,44] In the present study, aqueous carbonation of calcium hydroxide ($Ca(OH)_2$) using concentrated slurries (1 mol/L or 74 g/L) was preferentially investigated. The general investigated reaction can be written as follows:

$$Ca(OH)_2 + CO_{2(aq)} \rightarrow CaCO_{3(calcite)} + H_2O \quad (3)$$

DOI: 10.1021/acs.cgd.6b01406
Cryst. Growth Des. XXXX, XXX, XXX−XXX

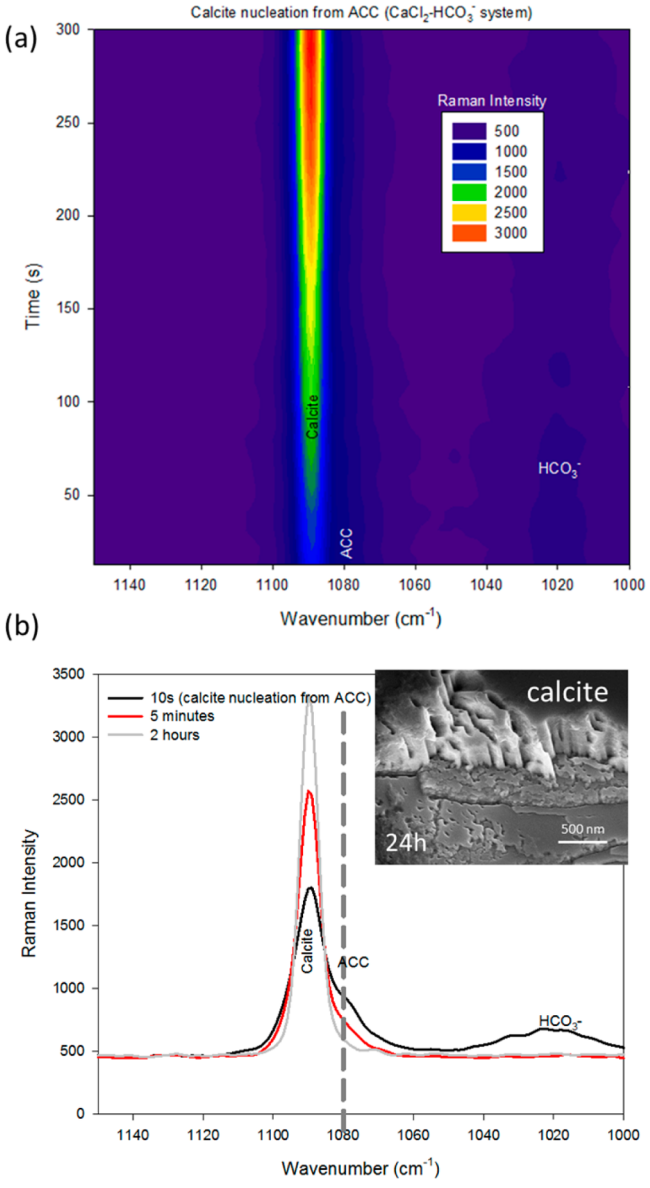

Figure 9. Nucleation and growth of calcite from ACC. (a) Time-resolved Raman spectroscopy monitoring of υ_1 intensity. (b) Residual ACC at 1078 cm^{-1} after 10 s of reaction and calcite peaking at 1089 cm^{-1} for three different reaction times. Inset shows a scanning electron microscopy image of calcite growing from ACC.

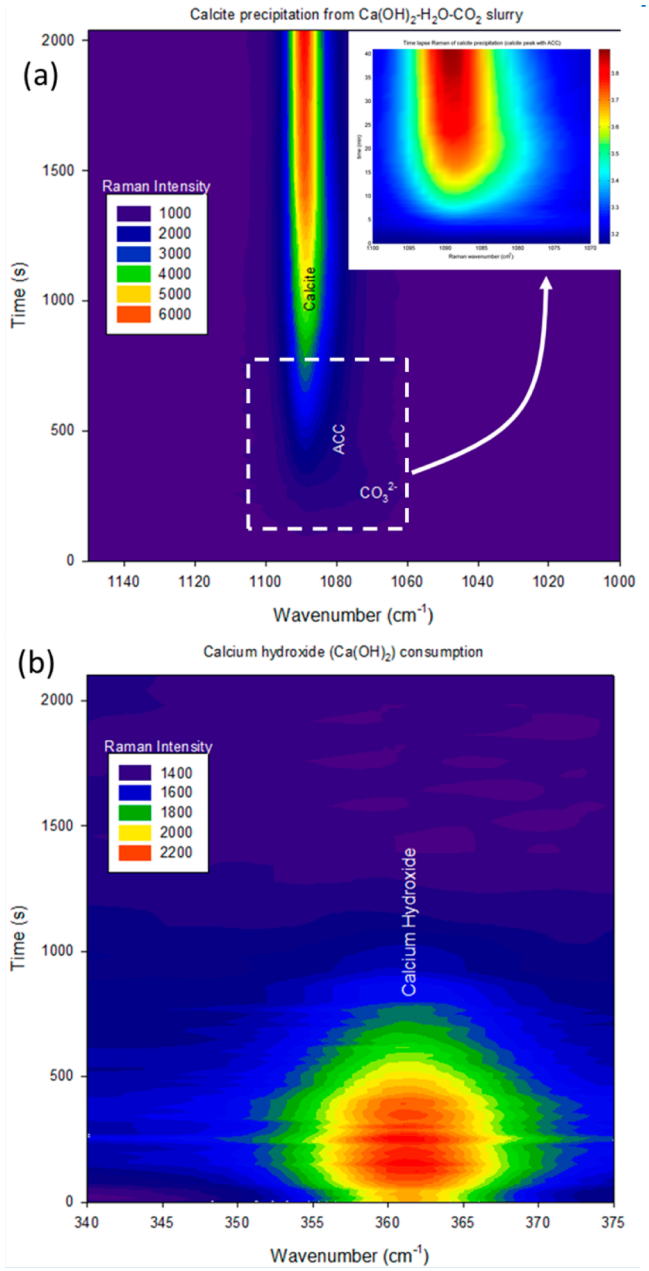

Figure 10. Time-resolved Raman spectroscopy monitoring of calcite nucleation from $Ca(OH)_2$–H_2O–CO_2 slurry at 25 °C with compressed CO_2 (initial pressure = 50 bar). (a) υ_1 vibrational mode for calcite (1089 cm^{-1}) and ACC (1079 cm^{-1}) and (b) calcium hydroxide consumption (362 cm^{-1}) during calcite formation.

As suggested in previous studies,[25,41] the absorption of CO_2 is the limiting step for carbonation of available calcium hydroxide ($Ca(OH)_2$). Note that calcium hydroxide is initially present in large excess (74 g/L or 1 mol/L) with respect to its solubility (1.73 g/L at 20 °C), and consequently this strong base maintains a high pH (>12) after CO_2 injection until it is completely transformed or carbonated after a given time t_c. This critical time corresponds to a sudden drop in pH during the experiments.[41] In practice, calcium hydroxide is completely consumed in the first 20 min by a carbonation process at 25 °C, as attested by Raman monitoring (see Figure 10b). Under these particular conditions, it is possible to determine whether calcium carbonate clusters and/or ACC are formed prior to calcite growth. Calcium carbonate nucleation is clearly detected after about 3 min of reaction (i.e., 3 min after CO_2 injection in the system), as demonstrated by the clear appearance of two υ_1 vibration modes, characteristic of the carbonate group, one peaking at 1087 cm^{-1} attributed to calcium carbonate and the other peaking at 1073 cm^{-1}, this latter probably related to complexe carbonate ions given that a single carbonate ion (CO_3^{2-}) peaks at 1069 cm^{-1} in the measuring instrument used. This first nucleation step probably involves calcium carbonate clusters because the lattice vibration modes for calcite, vaterite, or aragonite were not detected at this time. In fact, lattice vibration modes for calcite were exclusively detected after 5 min of reaction. Prior to this second nucleation event ($3 < t < 5$ min), ACC is present (slight bump at 1079 cm^{-1}) and coexists with calcite for about 2 min (Figure 11). After calcite nucleation ($t = 5$ min), calcite growth and eventually the nucleation

DOI: 10.1021/acs.cgd.6b01406
Cryst. Growth Des. XXXX, XXX, XXX−XXX

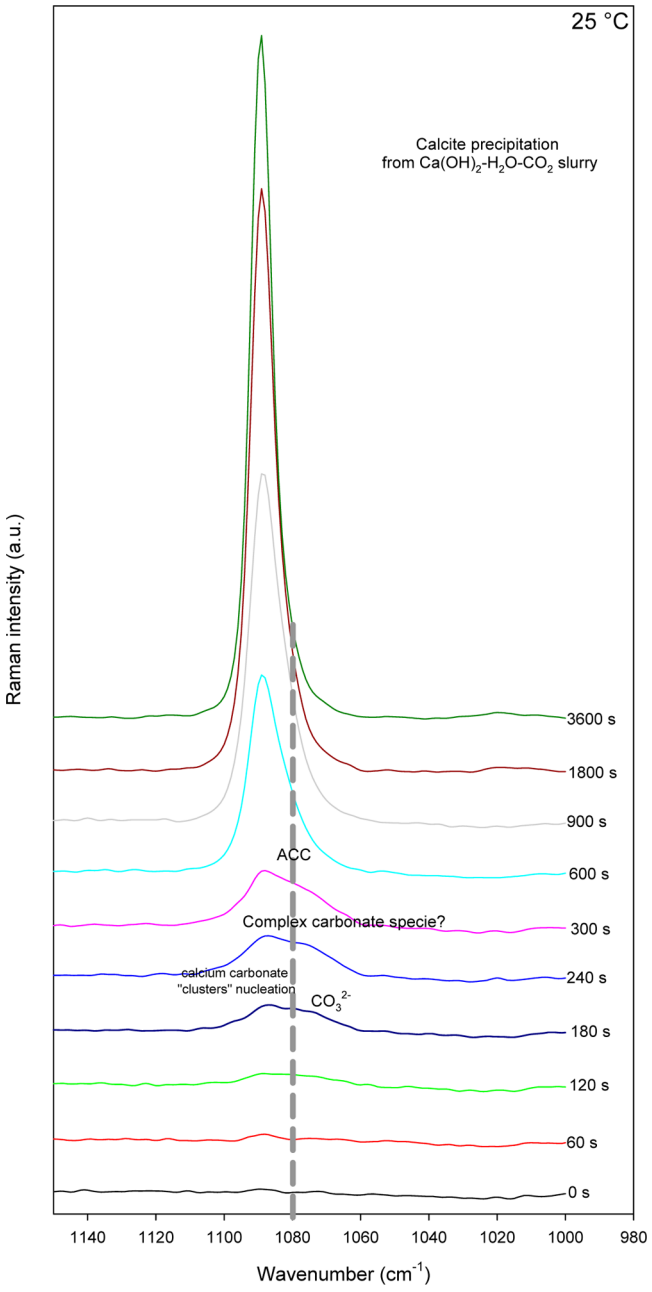

Figure 11. Raman spectra at different reaction times for calcite formation from $Ca(OH)_2$–H_2O–CO_2 slurry at 25 °C with compressed CO_2 (initial pressure = 50 bar). CO_3^{2-} carbonate species (~1072 cm^{-1}) and probably calcium carbonate clusters (1087 cm^{-1}) formed in situ after about 180 s. Moreover, it is also suspected that ACC forms after 300 s of reaction in the system.

of new calcite particles remain active processes until the complete consumption of calcium hydroxide, i.e., after about 20 min of reaction (see Figure 10 and Figure 12). When calcium hydroxide is completely consumed in the system, calcite grows by an Ostwald ripening process at 25 °C for 24 h, as suggested by a progressive thinning of all calcite vibrational modes, but reaching a spectroscopic equilibrium (not more significant variation of Raman intensity) after about 2 h of reaction. This is also supported by the integrated peaks for calcite that reach equilibrium after about 2 h (Figure 12). In this particular case, oriented aggregation of calcite nanoparticles is excluded, except when organic additives are used.[41]

4. IMPLICATIONS AND CONCLUDING REMARKS

The present study has demonstrated that time-resolved Raman spectroscopy in batch reactor experimental conditions offers new possibilities for investigating mineral condensation from ionic solutions and slurries, with direct relevance for industrial and environmental applications (wastewater treatment, protein purification, synthesis of nanoparticles and/or nanostructured materials, capture and transformation of CO_2, mineral processing). This powerful lab-based tool also provides basic knowledge to study the classical or nonclassical crystallization pathways in homogeneous or heterogeneous systems, the existence and persistence of precursors, transient phases during nucleation processes, and the role of organic matter in bioassisted systems. For example, the present study provides detailed reaction mechanisms and kinetics during nucleation and growth of siderite, calcite, and magnesite and the role of their precursors.

It is worth noting that magnesite is of particular interest for the permanent sequestration of CO_2 if magnesium is extracted from serpentines or olivine-rich ultrabasic rocks.[8,34] In this study, various scenarios were explored in order to understand the role of amorphous or crystalline precursors and their transformation to more stable phases was monitored in real-time at ambient temperature. As expected, the formation of amorphous precursors provides low energy pathways for crystallization of calcite and siderite, and, in this case, the crystals grow by oriented aggregation as revealed by FESEM ex situ observations on the final precipitates. Conversely, magnesite was not directly crystallized from AMC at ambient temperature. In fact, magnesite nucleation requires a higher temperature (T > 50 °C). In this context, the effects of a heat-aging step, solution chemistry, and reaction duration were assessed. It was clearly demonstrated that crystalline phases (not necessarily polymorphs) can also act as precursors and not only as inhibitors; this is the case for the nucleation of dypingite preceded by nesquehonite at ambient temperature (~25 °C) and for the nucleation of magnesite preceded by hydromagnesite at 50 and 90 °C. This means that the use of NaOH as CO_2 capturing agent enables the synthesis of magnesite (more stable magnesium carbonate) from brucite carbonation at moderate temperature.

On the other hand, the present study also provides complementary and new information on the mechanism of calcite formation from $Ca(OH)_2$–H_2O–CO_2 concentrated slurry. Here, Raman monitoring confirms that vaterite and aragonite polymorphs are absent during calcite nucleation at ambient temperature; however, calcium carbonate clusters and probably also ACC were detected in the first 5 min prior to calcite nucleation after about 5 min of reaction. Calcite growth was then nourished by consumption of calcium hydroxide for about 20 min followed by an Ostwald ripening mechanism for 2 h at ambient temperature. Assuming that the formation of ACC is not a significant step and that vaterite and aragonite are also absent, the calcite formation from $Ca(OH)_2$–H_2O–CO_2 concentrated slurry with high CO_2 pressure (initial P_{CO_2} = 50 bar) can be explained and numerically simulated by a classical crystallization pathway, as previously reported.[25] However, the in situ Raman detection of calcium carbonate clusters and ACC during calcite formation from $Ca(OH)_2$–H_2O–CO_2 concentrated slurry complements previous studies where these first

DOI: 10.1021/acs.cgd.6b01406
Cryst. Growth Des. XXXX, XXX, XXX−XXX

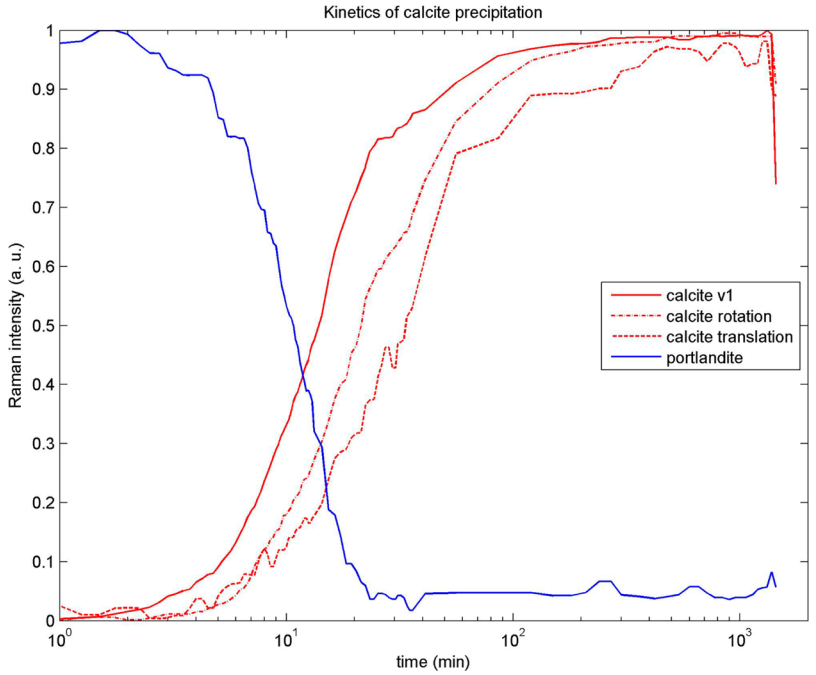

Figure 12. Kinetics of calcite nucleation and growth followed by integration of υ_1 and lattice vibrational mode peaks. Calcite growth and probably also nucleation of new particles nourished by portlandite ($Ca(OH)_2$ consumption in the first 20 min.

precipitating particles were not identified using ex situ solid characterizations in collected-time samples.

AUTHOR INFORMATION

Corresponding Author

*E-mail: german.montes-hernandez@ujf-grenoble.fr.

ORCID

German Montes-Hernandez: 0000-0002-8655-6530

Notes

The authors declare no competing financial interest.

ACKNOWLEDGMENTS

The authors acknowledge funding from the French National Centre for Scientific Research (CNRS), the Université Grenoble Alpes, the Labex OSUG@2020 (Investissement d'avenir-ANR10-LABX56) and GDF-Suez. Mineralogy and Geochemistry groups at ISTerre are also thanked for their contribution in the Raman funding.

REFERENCES

(1) Paquette, J.; Reeder, R. J. Relationship between surface structure, growth mechanism, and trace element incorporation in calcite. *Geochim. Cosmochim. Acta* **1995**, *59*, 735−749.

(2) Stipp, S. L. S.; Christensen, J. T.; Lakshtanov, L. Z.; Baker, J. A.; Waight, T. Rare Earth element (REE) incorporation in natural calcite: upper limits for actinide uptake in a secondary phase. *Radiochim. Acta* **2006**, *94*, 523−528.

(3) Kim, Y. Y.; Ribeiro, L.; Maillot, F.; Ward, O.; Eichhorn, S. J.; Meldrum, F. C. Bio-inspired synthesis and mechanical properties of calcite-polymer particle composite. *Adv. Mater.* **2010**, *22*, 1−5.

(4) Jimenez-Lopez, C.; Romanek, C. Precipitation kinetics and carbon isotope partitioning of inorganic siderite at 25°C and 1 atm. *Geochim. Cosmochim. Acta* **2004**, *68*, 557−571.

(5) Lim, D. I.; Jung, H. S.; Yang, S. Y.; Yoo, H. S. Sequential growth of early diagenetic freshwater siderites in the Holocene coastal deposits, Korea. *Sediment. Geol.* **2004**, *169*, 107−120.

(6) Sel, O.; Radha, A. V.; Dideriksen, K.; Navrotsky, A. Amorphous iron (II) carbonate: Crystallization energetics and composition to other carbonate minerals related to CO_2 sequestration. *Geochim. Cosmochim. Acta* **2012**, *87*, 61−68.

(7) Felmy, A. R.; Qafoku, O.; Arey, B. W.; Kovarik, L.; Liu, J.; Perea, D.; Ilton, E. S. Enhancing magnesite formation at low temperature and high CO_2 pressure: The impact of seed crystals and minor components. *Chem. Geol.* **2015**, *395*, 119−125.

(8) Hänchen, M.; Prigiobbe, V.; Baciocchi, R.; Mazzotti, M. Precipitation in the Mg-carbonate system-effects of temperature and CO_2 pressure. *Chem. Eng. Sci.* **2008**, *63*, 1012−1028.

(9) Wray, J. J.; Murchie, S. L.; Bishop, J. L.; Ehlmann, B. L.; Milliken, R. E.; Wilhelm, M. B.; Seelos, K. D.; Chojnacki, M. Orbital evidence for more widespread carbonate-bearing rocks on Mars. *J. Geophys. Res. (Planets)* **2016**, *121*, 652−677.

(10) Romanek, C. S.; Grady, M. M.; Wright, I. P.; Mittlefehldt, D. W.; Socki, R. A.; Pillinger, C. T.; Gibson, E. K., Jr. Record of fluid-rock interactions on Mars from the meteorite ALH84001. *Nature* **1994**, *372*, 655−657.

(11) Morse, J. W.; Casey, W. H. Ostwald processes and mineral paragenesis in sediments. *Am. J. Sci.* **1988**, *288*, 537−560.

(12) Navrotsky, A. Progress and new directions in high temperature calorimetry revisited. *Phys. Chem. Miner.* **1997**, *24*, 222−241.

(13) Lackner, K. Carbonate chemistry for sequestering fossil carbon. *Annu. Rev. Energy Environ.* **2002**, *27*, 193−232.

(14) Montes-Hernandez, G.; Fernandez-Martinez, A.; Charlet, L.; Tisserand, D.; Renard, R. Textural properties of synthetic calcite produced by hydrothermal carbonation of calcium hydroxide. *J. Cryst. Growth* **2008**, *310*, 2946−2953.

(15) Montes-Hernandez, G.; Perez-Lopez, R.; Renard, F.; Nieto, J. M.; Charlet, L. Mineral sequestration of CO_2 by aqueous carbonation of coal combustion fly-ash. *J. Hazard. Mater.* **2009**, *161*, 1347−1354.

(16) Smeets, P. J.; Cho, K. R.; Kempen, R. G.; Sommerdijk, N. A. J. M.; De Yoreo, J. J. Calcium carbonate nucleation driven by ion binding in a biomimetic matrix revealed by in situ electron microcopy. *Nat. Mater.* **2015**, *14*, 394−399.

(17) Nancollas, G. H.; Reddy, M. M. The crystallization of calcium carbonate II: calcite growth mechanism. *J. Colloid Interface Sci.* **1971**, *37*, 824−830.

DOI: 10.1021/acs.cgd.6b01406
Cryst. Growth Des. XXXX, XXX, XXX−XXX

(18) Teng, H. H.; Dove, P. M.; Orme, C. A.; De Yoreo, J. J. Thermodynamics of calcite growth: Baseline for understanding biomineral formation. *Science* **1998**, *282*, 724−727.
(19) Gebauer, D.; Völkel, A.; Cölfen, H. Stable prenucleation calcium carbonate clusters. *Science* **2008**, *322*, 1819−1822.
(20) Hu, Q.; Nielsen, M. H.; Freeman, C. L.; Hamm, L. M.; Tao, J.; Lee, J. R. I.; Han, T. Y. J.; Becker, U.; Harding, J. H.; Dove, P. M.; De Yoreo, J. J. The thermodynamics of calcite nucleation at organic interfaces: Classical vs. non-classical pathways. *Faraday Discuss.* **2012**, *159*, 509−523.
(21) Dideriksen, K.; Frandsen, C.; Bovet, N.; Wallace, A. F.; Sel, O.; Arbour, T.; Navrotsky, A.; De Yoreo, J. J.; Banfield, J. F. Formation and transformation of a short range ordered iron carbonate precursor. *Geochim. Cosmochim. Acta* **2015**, *164*, 94−109.
(22) Montes-Hernandez, G.; Renard, F.; Chiriac, R.; Findling, N.; Toche, F. Rapid precipitation of magnesite micro-crystals from $Mg(OH)_2$-H_2O-CO_2 slurry enhanced by NaOH and a heat-ageing step (from ∼ 20 to 90°C). *Cryst. Growth Des.* **2012**, *12*, 5233−5240.
(23) Song, R. Q.; Xu, A. W.; Antonietti, M.; Cölfen, H. Calcite crystals with platonic shapes and minimal surfaces. *Angew. Chem., Int. Ed.* **2009**, *48*, 395−399.
(24) Giuffre, A. J.; Hamm, L. M.; Han, N.; De Yoreo, J. J.; Dove, P. M. Polycacharide chemistry regulates kinetics of calcite nucleation through competition of interfacial energies. *Proc. Natl. Acad. Sci. U. S. A.* **2013**, *110*, 9261−9266.
(25) Fritz, B.; Clément, A.; Montes-Hernandez, G.; Noguera, C. Calcite formation by hydrothermal carbonation of portlandite: complementary insights from experiment and simulation. *CrystEngComm* **2013**, *15*, 3392−3401.
(26) Gower, L. B.; Tirrell, D. A. Calcium carbonate films and helices grown in solution of poly (aspartate). *J. Cryst. Growth* **1998**, *191*, 153−160.
(27) Gebauer, D.; Kellermeier, M.; Gale, J. D.; Bergstrom, L.; Colfen, H. Pre-nucleation clusters as solute precursors in crystallization. *Chem. Soc. Rev.* **2014**, *43*, 2348−2371.
(28) Wang, T.; Cölfen, H.; Antonietti, M. Nonclassical crystallization: Mesocrystals and morphology change of $CaCO_3$ crystals in the presence of a polyelectrolyte additive. *J. Am. Chem. Soc.* **2005**, *127*, 3246−3247.
(29) Wang, T.; Antonietti, M.; Cölfen, H. Calcite mesocrystals: "Morphing" crystals by a polyelectrolyte. *Chem. - Eur. J.* **2006**, *12*, 5722−5730.
(30) Song, R. Q.; Cölfen, H. Mesocrystals-Ordered Nanoparticle superstructures. *Adv. Mater.* **2010**, *22*, 1301−1330.
(31) Montes-Hernandez, G.; Chiriac, R.; Findling, N.; Toche, F.; Renard, F. Synthesis of Ceria (CeO_2 and CeO_{2-x}) Nanoparticles via Decarbonation and Ce(III) Oxydation of Synthetic Bastnäsite (CeCO3F). *Mater. Chem. Phys.* **2016**, *172*, 202−210.
(32) Hamm, L. M.; Giuffre, A. J.; Han, N.; Tao, J.; Wang, D.; De Yoreo, J. J.; Dove, P. M. Reconciling disparate views of template-directed nucleation through measurement of calcite nucleation kinetics and binding energies. *Proc. Natl. Acad. Sci. U. S. A.* **2014**, *111*, 1304.
(33) Swanson, E. J.; Fricker, K. J.; Sun, M.; Park, A. H. Directed precipitation of hydrated and anhydrous magnesium carbonates for carbon storage. *Phys. Chem. Chem. Phys.* **2014**, *16*, 23440−23450.
(34) Qafoku, O.; Dixon, A.; Rosso, K. M.; Schaef, H. T.; Bowden, M. E.; Arey, B. W.; Felmy, A. R. Dynamics of magnesite formation at low temperature and high pCO_2 in aqueous solution. *Environ. Sci. Technol.* **2015**, *49*, 10736−10744.
(35) Deelman, J. C. Breaking Ostwald's rule. *Chem. Erde-Geochem.* **2001**, *61*, 224−235.
(36) Pimentel, C.; Pina, C. M. The formation of the dolomite-analogue norsethite: Reaction pathway and cation ordering. *Geochim. Cosmochim. Acta* **2014**, *142*, 217−223.
(37) Xu, J.; Yan, C.; Zhang, F.; Konishi, H.; Xu, H.; Teng, H. Testing the cation-hydration effect on the crystallization of Ca-Mg-CO_3 systems. *Proc. Natl. Acad. Sci. U. S. A.* **2013**, *110*, 17750.
(38) Dey, A.; de With, G.; Sommerdijk, N. A. J. M. In situ techniques in biomimetic mineralization studies of calcium carbonate. *Chem. Soc. Rev.* **2010**, *39*, 397−409.
(39) Louvel, M.; Bordage, A.; Da Silva-Cadoux, C.; Testemale, D.; Lahera, E.; Del Net, W.; Geaymond, O.; Dubessy, J.; Argoud, R.; Hazemann, J. L. A high-pressure high-temperature setup for in situ Raman spectroscopy of supercritical fluids. *J. Mol. Liq.* **2015**, *205*, 54−60.
(40) Truche, L.; Bazarkina, E. F.; Berger, G.; Caumon, M. C.; Bessaque, G.; Dubessy, J. Direct measurement of CO_2 solubility and pH in NaCl hydrothermal solutions by combining in situ potentiometry and Raman spectroscopy up to 280°C and 150°C. *Geochim. Cosmochim. Acta* **2016**, *177*, 238−253.
(41) Montes-Hernandez, G.; Renard, F.; Findling, N.; Auzende, A. L. Formation of porous calcite mesocrystals from CO_2-H_2O-$Ca(OH)_2$ slurry in the presence of common domestic drinks. *CrystEngComm* **2015**, *17*, 5725−5733.
(42) Montes-Hernandez, G.; Findling, N.; Renard, R.; Auzende, A. L. Precipitation of ordered dolomite via simultaneous dissolution of calcite and magnesite: New experimental insights into an old precipitation enigma. *Cryst. Growth Des.* **2014**, *14*, 671−677.
(43) Wallace, A. F.; Hedges, L. O.; Fernandez-Martinez, A.; Raiteri, P.; Gale, J. D.; Waychunas, G. A.; Whitelam, S.; Banfield, J. F.; De Yoreo, J. J. Microscopic Evidence for liquid-liquid separation in supersaturated $CaCO_3$ solutions. *Science* **2013**, *341*, 885−889.
(44) Demichelis, R.; Raiteri, P.; Gale, J. D.; Quigley, D.; Gebauer, D. Stable prenucleation mineral clusters are liquid-like ionic polymers. *Nat. Commun.* **2011**, *2*, 590.

DOI: 10.1021/acs.cgd.6b01406
Cryst. Growth Des. XXXX, XXX, XXX−XXX